Neuron, Vol. 45, 133–145, January 6, 2005, Copyright ©2005 by Elsevier Inc. DOI 10.1016/j.neuron.2004.12.024

# Direction Selectivity of Excitation and Inhibition in Simple Cells of the Cat Primary Visual Cortex

**Nicholas J. Priebe* and David Ferster**
Department of Neurobiology and Physiology
Northwestern University
Evanston, Illinois 60208

## Summary

**Direction selectivity in simple cells of primary visual cortex, defined from their spike responses, cannot be predicted using linear models. It has been suggested that the shunting inhibition evoked by visual stimulation is responsible for the nonlinear component of direction selectivity. Cortical inhibition would suppress a neuron's firing when stimuli move in the nonpreferred direction, but would allow responses to stimuli in the preferred direction. Models of direction selectivity based solely on input from the lateral geniculate nucleus, however, propose that the nonlinear response is caused by spike threshold. By extracting excitatory and inhibitory components of synaptic inputs from intracellular records obtained in vivo, we demonstrate that excitation and inhibition are tuned for the same direction, but differ in relative timing. Further, membrane potential responses combine in a linear fashion. Spike threshold, however, quantitatively accounts for the nonlinear component of direction selectivity, amplifying the direction selectivity of spike output relative to that of synaptic inputs.**

## Introduction

Selectivity for the direction of visual motion requires a comparison of luminance or contrast cues across both space and time. It is known that this comparison is performed by neurons of the visual cortex, since the visual inputs to the cortex from relay cells of the lateral geniculate nucleus (LGN) are almost completely insensitive to direction. Two fundamentally different models of the visual cortex have emerged to explain the origin of cortical direction selectivity. In the first model, cortical neurons compare the visual image across both space and time by integrating excitatory inputs of different response latencies and offset receptive field positions (DeAngelis et al., 1993; Emerson, 1997; Emerson and Huang, 1997; McLean and Palmer, 1989; McLean et al., 1994; Reid et al., 1987, 1991). Saul and Humphrey have provided evidence that the inputs with fast and slow latencies correspond to nonlagged and lagged relay cells of the LGN (Jagadeesh et al., 1993; Saul and Humphrey, 1990, 1992). If synaptic inputs from lagged and nonlagged cells were segregated within each ON and OFF subfield of a simple cell, the resulting spatial gradients of response latency would make the cell prefer motion in the direction of decreasing latency. That is, a motion-selective neuron will receive simultaneous and therefore maximal excitation from all regions of its receptive field only when the different parts are activated in the proper order by a moving stimulus, starting from the slowest latency region and proceeding to the fastest.

In a second set of models, the spatiotemporal organization of the excitatory input does not account for direction selectivity (Barlow and Levick, 1965; Torre and Poggio, 1978). Instead, spatially offset, long-lasting inhibition suppresses the responses to the nonpreferred direction. These two models differ substantially: the first model predicts that excitation (that is, the aggregate excitation from all inputs) would be tuned for the preferred direction; the second predicts that neither excitation nor inhibition is, by itself, tuned for motion direction. Only their interaction gives rise to direction selectivity.

Most models of motion selectivity require a nonlinear process to sharpen selectivity relative to selectivity of the excitatory synaptic inputs. Linear estimates of the cortical direction selectivity generally underestimate true direction selectivity (Baker, 2001; DeAngelis et al., 1993; Emerson and Huang, 1997; Reid et al., 1987, 1991) but may be corrected by adding a nonlinear step, such as a threshold or squaring (DeAngelis et al., 1993; Emerson and Huang, 1997). There is some evidence that this nonlinearity is generated by spike threshold, since the subthreshold modulations in membrane potential are under some circumstances highly linear in direction-selective cells, much more so than the spike output of the cells (Jagadeesh et al., 1993, 1997). A second possible nonlinear mechanism underlying direction selectivity is shunting inhibition. In Torre and Poggio's (Torre and Poggio, 1978) model, for example, the inhibition evoked by stimuli moving in the nonpreferred direction takes the form of a shunt, which would nonlinearly suppress any excitation evoked by the stimuli. The discovery of strong, visually evoked shunting inhibition in direction-selective retinal cells (Grzywacz and Koch, 1987) and in cortical cells (Anderson et al., 1999; BorgGraham et al., 1998; Hirsch et al., 1998) strengthens the possibility that shunting inhibition plays a role in the origin of direction selectivity.

To explore the role of inhibition, both shunting and hyperpolarizing, in cortical direction selectivity, we have recorded intracellularly in vivo from cortical simple cells and measured the direction selectivity of excitatory and inhibitory synaptic inputs. Direction selectivity was assessed from the voltage response to drifting sinusoidal gratings, as well as voltage responses to bright and dark bars flashed randomly within the neuron's receptive field (1D noise). Excitatory and inhibitory inputs were distinguished by recording voltage responses while injecting hyperpolarizing current of different amplitudes into the cell. Cesium and QX-314 were used in some cases to block voltage-gated currents. We have found that excitation and inhibition were tuned to the same direction of motion: motion of a grating stimulus in the preferred direction elicited both the largest excitatory and the largest inhibitory inputs onto simple cells (Ferster, 1986; Monier et al., 2003). Inhibition and excitation evoked by motion in the preferred direction, however, were temporally out of phase with one another. In addition, the

*Correspondence: nico@northwestern.edu

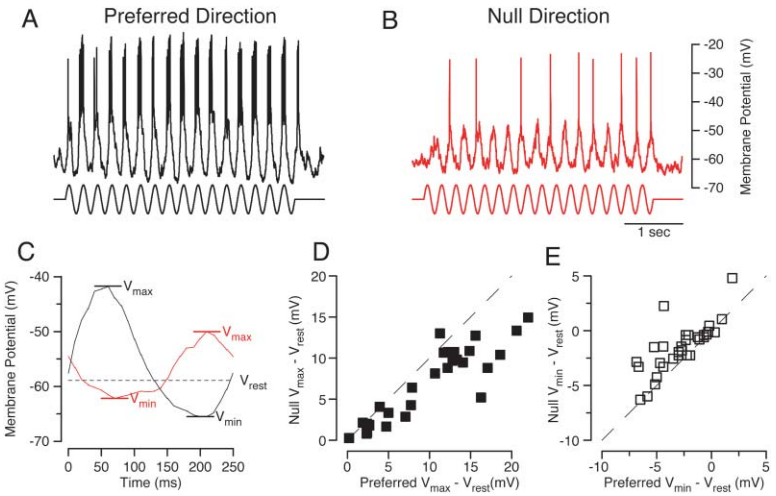


**Figure 1. The Direction Selectivity of Simple Cells in Primary Visual Cortex**

The membrane potential of a direction-selective neuron responding to a sinusoidal grating moving in the preferred direction (A) or the opposite (null) direction (B). The solid trace below the potential traces illustrates the temporal frequency of the grating. (C) Cycle averages of the response to the grating motion in the preferred direction (black trace) and null direction (red trace). $V_{max}$ and $V_{min}$ were extracted from the peak and trough of the potential responses. $V_{rest}$ is the average potential to a gray screen. Scattergrams illustrate the difference of $V_{max}$ (D) or $V_{min}$ (E) from $V_{rest}$ across the population of V1 neurons for the preferred and null direction. Each symbol represents an individual neuron.

spatial gradient of response latency for excitation and inhibition, as measured from the noise stimuli, accounted quantitatively for the direction selectivity as measured from the responses to gratings. Using a linear combination of the synaptic inputs derived from the noise stimuli, followed by an expansive threshold nonlinearity, the direction selectivity of both membrane potential and spike responses could be accurately predicted. There was little indication that inhibition in the null direction, either of the shunting or hyperpolarizing kind, contributes to the direction selectivity of simple cells.

## Results

### Direction-Selective Responses to Grating Stimulation

We made in vivo whole-cell intracellular recordings from 34 simple cells in cat area 17. Direction selectivity was measured from the response to drifting gratings of the preferred spatial frequency, temporal frequency, and orientation (Figures 1A and 1B). Direction selectivity was quantified using the direction index:

$$DI = \frac{(R_p - R_n)}{(R_p + R_n)} \quad (1)$$

where $R_p$ and $R_n$ are the amplitudes of the modulated (F1) component of the response (membrane potential or spike rate) to gratings of the preferred and nonpreferred directions. Although the spiking response of neurons was often highly selective for the direction of motion, the membrane potential modulation of the response was less selective (Jagadeesh et al., 1993, 1997). For the neuron shown in Figure 1, the spiking response of the neuron was almost completely selective for motion direction ($DI = 0.82$), while the voltage response was only modestly selective ($DI = 0.36$). Across our population of neurons, the direction index derived from spiking was two to three times the direction index derived from membrane potential (see below).

By definition, motion in the preferred direction caused a larger peak-to-peak modulation of the membrane potential than motion in the null direction. From the cycle averages of these responses (Figure 1C), we also found that motion in the preferred direction evoked both a larger maximum depolarization ($V_{max}$) and a larger maximum hyperpolarization ($V_{min}$) than were evoked by motion in the nonpreferred direction. This was largely the case across our population when measured relative to each neuron's resting potential ($V_{rest}$). In Figure 1D, maximum depolarization ($V_{max} - V_{rest}$) for the null stimulus is plotted against maximum depolarization for the preferred stimulus, and the points tend to fall below the unity line. Similarly, when minimum hyperpolarization ($V_{min} - V_{rest}$) for the null stimulus is plotted against maximum hyperpolarization for the preferred stimulus (Figure 1E), the points tend to fall above the unity line. The average difference between the $V_{max} - V_{rest}$ for the preferred and opposite directions was 3.1 mV ($\pm$0.53, t test, $p < 0.05$), while the average difference between $V_{min} - V_{rest}$ for the preferred and opposite directions was $-$1.4 mV ($\pm$0.28, t test, $p < 0.05$).

There are a number of possible sources for the hyperpolarizing phase of the membrane potential response to grating motion. It could result directly from synaptic inputs, either an increase in inhibition above the resting level or a decrease in excitation below the resting level. Alternatively, the hyperpolarization could be a secondary effect of the depolarizing phase of the grating response. For example, the barrage of spikes that occurs during the depolarizing phase could evoke a delayed afterhyperpolarization through the opening of voltage-gated potassium channels (McCormick et al., 1985). If afterhyperpolarization were the cause of the hyperpolarization, the amplitude of the hyperpolarization ($V_{min}$) should be correlated with the number of spikes that occurred in the preceding depolarization. Therefore, in each cell we measured $V_{min}$ from stimulus cycles in which the preceding depolarization did not trigger any spiking. Even when calculated from this restricted set of data, the average $V_{min} - V_{rest}$ for the preferred direction of motion ($-$2.59) was still more hyperpolarized than $V_{min} - V_{rest}$ for the null direction ($-$1.33), suggesting that the selectivity of $V_{min}$ for the preferred direction of motion is synaptic in origin.

To examine the excitatory and inhibitory synaptic inputs to direction-selective neurons more directly, we derived estimates of the excitatory and inhibitory synap-

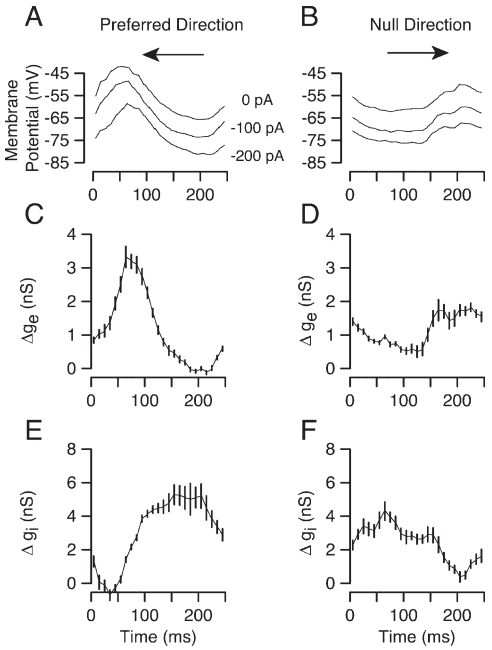


Figure 2. Excitatory and Inhibitory Conductances in a Direction-Selective Neuron

Membrane potential responses to the preferred (A) and null (B) direction are shown under three different conditions of current injection (0, −100, and, −200 pA). Excitatory conductances for the preferred (C) and null direction (D) and inhibitory conductances for the preferred (E) and null direction (F) were extracted from the cycle-averaged responses to moving gratings. Error bars indicate 95% confidence intervals computed using a bootstrap technique (Sokal and Rohlf, 1995).

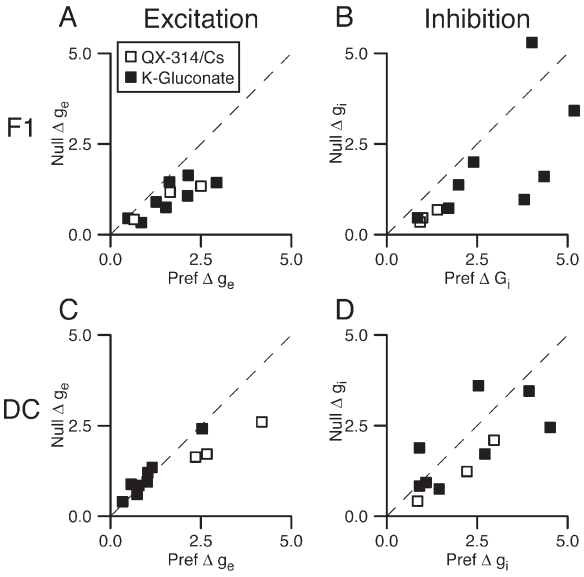


Figure 3. The Tuning of Excitation and Inhibition in Direction-Selective Neurons

The modulation amplitude (F1) for excitatory conductance (A) or inhibitory conductance (B) are plotted for preferred and null stimulus conditions. The mean amplitude (DC) of excitatory conductance (C) and inhibitory conductance (D) are plotted for the preferred and null directions. Open symbols refer to neurons recorded with a $Cs^+$-methanesulfonate-based solution and QX-314. Closed symbols indicate neurons recorded with the standard $K^+$-gluconate solution.

tic conductances by measuring the voltage response of the neuron while injecting steady currents of different amplitudes through the recording electrode (Figures 2A and 2B). Hyperpolarizing currents were used primarily to avoid activating voltage-dependent currents associated with spiking. Correction for electrode series resistance (bridge balance) was performed offline with double exponential fits to the responses to injected current steps (Anderson et al., 2000a). The values of $I$ (injected current), $V_m$, and $dV_m/dt$ measured at each moment in time were applied to the membrane equation (see Experimental Procedures and the Supplemental Data for details [http://www.neuron.org/cgi/content/full/45/1/133/DC1/]). $\Delta g_e$ and $\Delta g_i$, the visually evoked changes in excitatory and inhibitory conductances (measured relative to resting conductance), are shown in Figures 2C–2F. As a measure of the accuracy of the derived conductances, the conductances were used to rederive the membrane potential. Substantial nonlinearities (such as voltage-gated conductances) would be detected as a mismatch between these derived potentials and the original recorded potentials, whereas the match between measurement and prediction was quite good (Figure 3 and Supplemental Data).

As has been shown previously (Anderson et al., 2000a), excitation and inhibition to simple cells are both modulated by the preferred grating, but at nearly opposite phases (Figures 2C and 2D). That is, the time of greatest inhibition was close to the time of the least excitation. For the example neuron in Figure 2, the phase difference between sine waves fitted to $\Delta g_e$, and $\Delta g_i$ is 143°. Although excitation and inhibition were both smaller for the nonpreferred stimulus than they were for the preferred stimulus, excitation and inhibition were again at nearly opposite phases (phase difference = 164°). Across the sample, the amplitude of the modulated component of excitation was larger in response to the preferred direction than the null direction in all cells ($n = 11$) in which conductance measurements were made (Figure 3A, paired t test, $p < 0.05$). The amplitude of the modulated component of inhibition was larger in response to the preferred direction in 10 out of the 11 cells (Figure 3B) (paired t test, $p < 0.05$).

Although the modulated components of excitation and inhibition clearly depended on the direction of motion, there were only slight differences between the mean (DC component) of the excitatory and inhibitory conductances evoked by the preferred and null directions (Figures 3C and 3D). The average difference between preferred- and null-evoked mean $\Delta g_i$ was 0.42 nS, which by t test is not significant ($p = 0.15$). The same is true for excitation (average difference in mean $\Delta g_e = 0.25$ nS; $p = 0.19$). Therefore, the total amount of inhibition (or excitation) evoked by the preferred stimulus differs little from that evoked by the null stimulus. Only the relative timing of excitation and inhibition depends on stimulus direction.

### Direction Selectivity from X-T Receptive Field Maps

To explore the spatiotemporal receptive field structure underlying direction selectivity of V1 simple cells, we

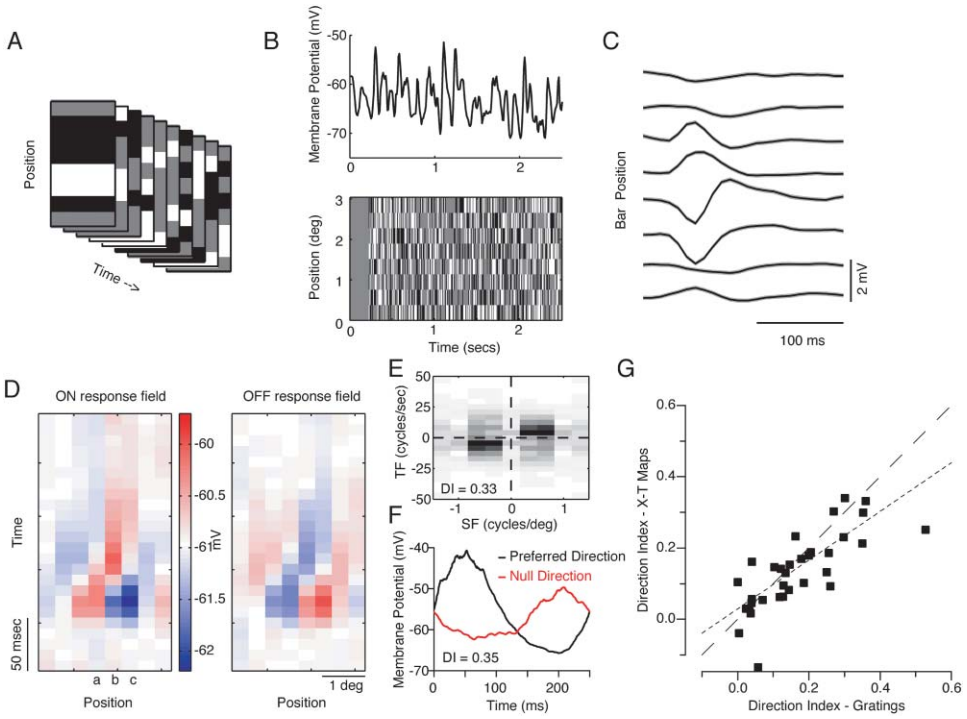


Figure 4. Using 1D Noise to Characterize Spatiotemporal Receptive Fields of Direction-Selective Neurons

Bars oriented in the preferred orientation were placed over the receptive field of V1 simple cells. (A) The luminance of each bar was randomly set to either light, gray, or dark at each frame. (B) Membrane potential (top trace) was recorded while presenting the 1D bar noise stimulus (bottom trace). (C) Average membrane potential after a light bar was presented at each bar location. Dark lines indicate the average response of the neuron, gray indicates the standard error of the mean. (D) Spatiotemporal representation of the average response after each light bar (left panel) or dark bar (right panel). The response after each bar has been presented is represented by each column, where the time of the bar presentation is at the bottom of the panel. Red indicates a membrane potential above the average potential during stimulation. Blue indicates a potential below the average membrane potential. (E) The 2D Fourier transform of the difference in the ON and OFF response fields shown in (D). Dark indicates increased energy. The increased energy in upper right and lower left quadrants are the signatures of a direction-selective response spatiotemporal filter (Adelson and Bergen, 1985; DeAngelis et al., 1993). The direction index was computed by comparing the total energy in the upper right quadrant to the energy in the lower right quadrant. (F) Cycle averages of the grating response of the same neuron. (G) A comparison of the membrane potential direction index computed from the responses to the 1D noise stimulation and the responses to moving gratings. Each symbol represents an individual neuron. The line composed of large dashes has a slope of 1 and a y-intercept of 0. The fine dashed line represents the linear regression of the data (slope = 0.69, y-intercept = 0.03).

presented 1D noise stimulus within each neuron's receptive field (Conway and Livingstone, 2003; DeAngelis et al., 1993; McLean and Palmer, 1989; McLean et al., 1994). The stimulus consisted of bars of the preferred orientation randomly and independently switched between dark, light, and gray (background) every 10 ms, that is, at each refresh of the video monitor (Figure 4A). Standard, stimulus-triggered averaging was applied to the membrane potential responses (Figure 4B) to calculate the average response to the light and dark bar flashed at each position. ON responses are shown in Figure 4C. Shading around each trace indicates the standard error of the response at each point in time. The same data are presented as a color-coded space-time map in Figure 4D (ON response field), together with a space-time map for the responses to dark stimuli (OFF response field). Depolarizations are shown in red, hyperpolarizations in blue. Both the ON and OFF response fields are tilted in space-time. For example, the latency of the peak depolarizing response evoked by a bright bar (Figure 4D) is about 60 ms at location "a," but shifts to almost 100 ms at location "c." This shift in response latency across the receptive field has been observed in extracellular recordings from direction-selective neurons and is thought to give rise to direction selectivity (Conway and Livingstone, 2003; DeAngelis et al., 1993; Emerson et al., 1987; Reid et al., 1991). If a light bar were successively moved at the appropriate speed from position "c" to "b" and finally to "a," the inputs from these three positions would reach the cell simultaneously and sum together to generate a large depolarization. If, however, the bar is moved in the opposite direction, from position "a" to "b" and finally to "c," the input from position "a" would arrive at the cell long before the inputs from "b" or "c." The asynchronous inputs from different locations would therefore sum to a relatively small peak depolarization which may not bring the neuron to spike threshold.

To quantify the degree of direction selectivity inherent in the spatiotemporal receptive fields, we first subtracted the OFF response field from the ON response field and then transformed the result into frequency space by applying a 2D Fourier transformation (Figure 4E). Energy contained within the upper right and lower left quadrants of the transform ($E_P$) is a measure of the rightward tilt in the spatiotemporal maps and therefore

corresponds to the cell's sensitivity to motion in one direction. Energy in the upper left and lower right quadrants ($E_N$) corresponds to leftward tilt in the maps and therefore to sensitivity to motion in the opposite direction (DeAngelis et al., 1993). It is possible to estimate the direction selectivity predicted by the spatial maps by calculating a direction index from the total energy in the two halves of the Fourier transform: $DI = (E_P - E_N)/(E_P + E_N)$. In the cell in Figure 1, for example, the predicted direction index is 0.33, which corresponds closely to the direction index of 0.35 measured from the membrane potential changes evoked by drifting gratings (Figure 1F). A similar match between the measured and predicted direction indices was observed across our sample of 31 simple cells in which this measurement was made (Figure 4G). The correlation between the measurement and prediction was high ($R^2 = 0.59$), and the slope of a linear regression was not significantly different from 1 (slope = 0.69, p = 0.09; y-intercept = 0.03, p = 0.22). That the direction selectivity measured with moving stimuli can be predicted from the response of cells to stationary flashing stimuli suggests that the cells are summing their synaptic inputs linearly (Jagadeesh et al., 1993, 1997).

### Linearity of Spatial Summation

To assess the linearity of each neuron's response further, we attempted to predict the response to each frame of the noise stimulus from a sum of the measured responses to each of its component bars. At every stimulus frame during the course of a noise stimulus, we determined which bars were either dark or bright. The corresponding average responses for each of these bars (as in Figure 4C) were added into the predicted trace, aligned on the time of occurrence of the bar. For each time, *t*, the value of the measured potential was then plotted against the predicted potential (Figure 5, right-hand column, black points). Superimposed on the scatter plot of instantaneous predicted and measured potentials is a running average of these points together with the standard deviation of the average (Figure 5, right-hand column, red curves). For the five cells shown, the relationship between the predicted potential and the average measured potential follows a nearly linear trajectory, with some saturation at both the high and low ends of the curve. In the linear portion of the curve, the predicted and measured potentials are very close to one another, yielding a slope close to 1. Thus, the linear predictions are quite accurate, suggesting that the cells are summing their inputs in a linear fashion. It is difficult to determine the exact causes of saturation in the curves, but at the high end, saturation could arise from the active conductances associated with threshold, and on the low end by reduction in the driving force for inhibitory currents. The vertical scatter of the points around the mean value is comparable in amplitude to the trial-to-trial noise in the response to a blank (mean luminance) screen.

### Direction Selectivity of Inhibition

One aspect of the responses shown in Figure 5 is that negative stimuli—stimuli that are anticorrelated with the spatiotemporal receptive field—evoked true hyperpolarizations from rest. In this case, it is important to note that a perfectly anticorrelated stimulus is not a stimulus moving in the nonpreferred direction, but instead is a stimulus moving in the preferred direction, but with dark pixels in the ON regions and bright pixels in the OFF regions of the spatiotemporal receptive field. The net hyperpolarization that such preferred direction stimuli evoke suggests that synaptic inhibition is tuned for the same direction as the synaptic excitation.

Although hyperpolarization and depolarization are often correlated with synaptic inhibition and excitation, there is not a one-to-one correlation, since hyperpolarization can be generated by a withdrawal of excitation, or, more rarely, depolarization can be caused by a withdrawal of inhibition. To extract a more accurate measure of the changes in excitatory and inhibitory conductances evoked by the noise stimuli, we used the same procedure used above for the grating responses, presenting the noise stimuli repeatedly while injecting currents of different amplitudes into the cell. Spatiotemporal receptive field maps were constructed both from the membrane potential, $V_m$, and from $dV_m/dt$ at different levels of current injection for application to the membrane equation (Equation 3, see Experimental Procedures and the Supplemental Data [http://www.neuron.org/cgi/content/full/45/1/133/DC1/]). ON and OFF maps for two cells recorded with 0 nA of current are shown in Figures 6A and 6B, together with derived maps for excitatory and inhibitory conductances. The maps show changes in conductance relative to the mean value recorded during the noise stimulus, which remained above the resting value during the course of the stimulus.

Spatiotemporal (x-t) maps of excitatory and inhibitory conductances both contain the characteristic tilt that underlies motion selectivity (Figure 6A), and like depolarization and hyerpolarization, excitation and inhibition are tilted in the same direction. As before, we quantified the direction selectivity of conductance maps by transforming the result in Fourier space and comparing the energy in one direction to the energy in the opposite direction. The cell in Figure 6A had a direction index of 0.27 for excitation and 0.33 for inhibition in response to light bars; the cell in Figure 6B had direction indices of 0.11 for excitation and 0.15 for inhibition. Direction indices for excitation are plotted against those for inhibition for all the cells in which reliable measurements could be obtained (Figure 7E). All points are in the upper half of the graph, indicating identical preferred directions, and many points fall near a line of slope 1, indicating similar degree of direction preference.

Despite the similarity in direction preference of excitation and inhibition, there was a striking distinction between the excitatory and inhibitory conductance maps: wherever there was an increase in the excitatory conductance, there tended to be a decrease in the inhibitory conductance. This is evident in both pairs of maps in Figure 6. Corresponding areas that are red in one map (indicating an increase relative to the average conductance) are blue in the other (decrease relative to the average conductance). A more direct comparison of excitation and inhibition is made in Figure 7D, which shows profiles through the excitatory and inhibitory maps at one position for a different cell (Figures 7A and 7B).

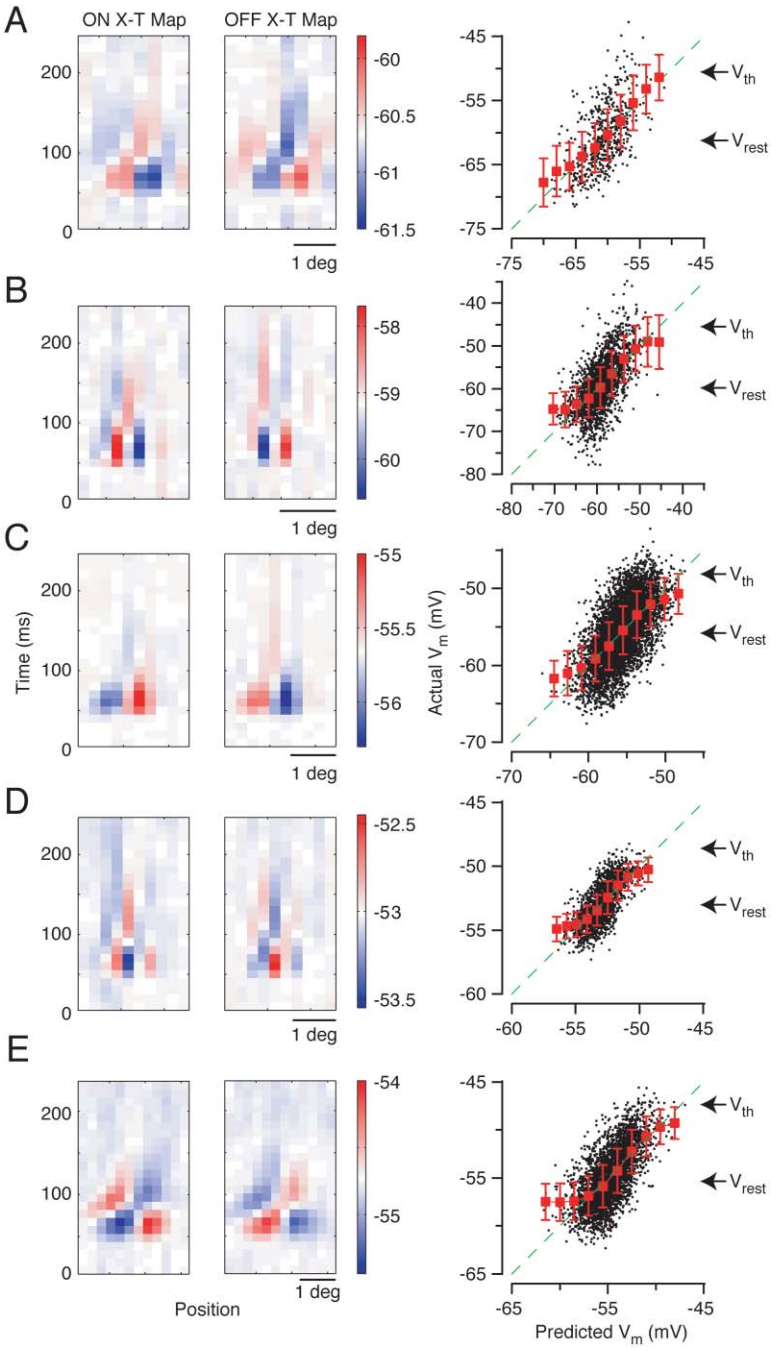


Figure 5. Spatiotemporal Receptive Fields of Direction-Selective Neurons

(A) The average membrane potential responses after the presentation of bright bars (left panel) or dark bars (middle panel) are indicated by a color. The right panel plots the relationship between the actual membrane potential and the membrane potential predicted by the convolution of the stimulus and the receptive fields in the left panels. Each point shows the actual and predicted membrane potential for a single monitor refresh (10 ms). The average membrane potential for different levels of predicted potential is shown by the red trace (error bars indicate standard deviation). The dashed green trace shows a line of slope of 1 and y-intercept of 0. (B–E) Panels follow the same format as in (A) for different example neurons.

Increases in inhibition occur more or less simultaneously with decreases in excitation, and vice versa.

We quantified the degree of overlap between excitation and inhibition by computing the cross-correlation between the elements in the excitatory and inhibitory maps. A rectangular region of the x-t conductance maps (outlined region in Figures 7A and 7B) was first constructed by finding those spatial positions with significant changes in conductance at any latency and those latencies with significant changes in conductance at any position. The correlation coefficient was then computed between the excitatory and inhibitory conductance maps in this restricted region. If the excitatory maps were the complete opposite of the inhibitory maps, the cross-correlation would be $-1$; for identical maps, the cross-correlation would be 1. A histogram of the cross-correlation for 11 cells is shown in Figure 7D (open bars, ON responses; closed bars, OFF responses). Note that all pairs of excitatory and inhibitory maps were negatively correlated (average cross correlation $= -0.56$). The negative correlations between space-time oriented maps suggest that excitation and inhibition are arranged in a push-pull fashion in space-time, just as they are in the spatial receptive fields of simple cells (Anderson et al., 2000a; Ferster et al., 1996; Ferster and Miller, 2000; Hirsch et al., 1998). ON excitation is accompanied by

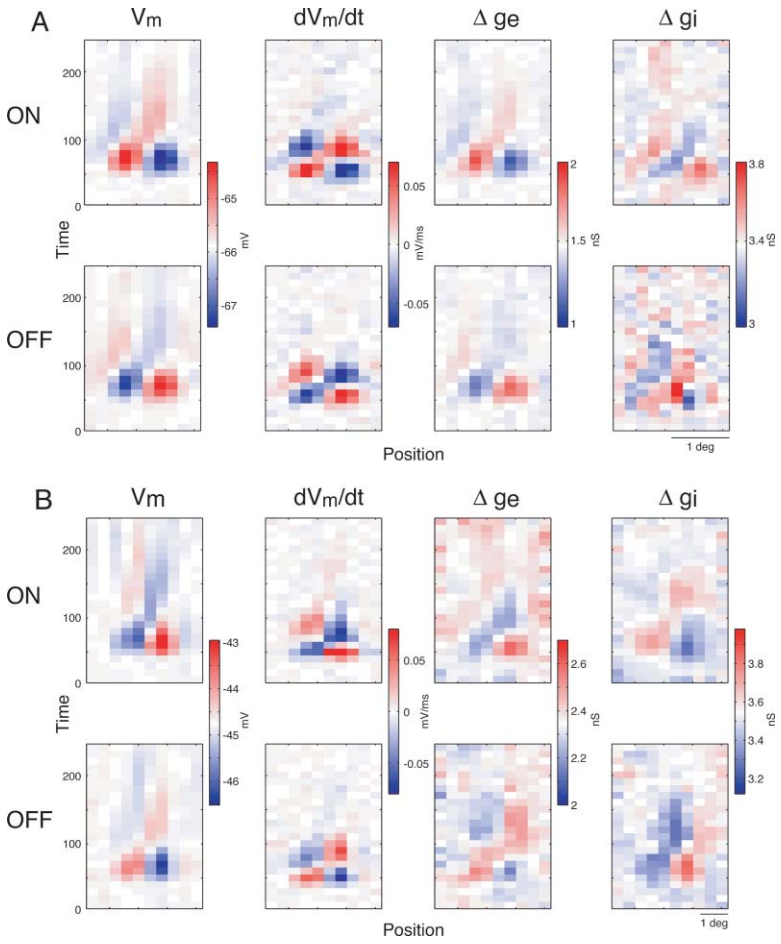


Figure 6. X-T Maps of Excitatory and Inhibitory Conductance

(A) The top row shows x-t maps for membrane potential, *dVm/dt*, $\Delta g_e$, and $\Delta g_i$ for bright bars for a single neuron. The maps follow the same convention used in Figure 5. The bottom row of x-t maps follows the same format, but the x-t maps correspond to the response to dark bars. (B) Same format as (A), for a different neuron.

OFF inhibition, and vice versa. We also measured the spatial extent of inhibitory and excitatory conductance, since some models postulate that motion selectivity is based on spatially and temporally offset inhibition and excitation (Barlow and Levick, 1965; Torre and Poggio, 1978). These models predict that inhibition should be located more on one side of the map than the other. We found little spatial structure in either the inhibitory or excitatory conductance when averaged over the epoch of significant conductance change, as shown for the neuron in Figure 7 (Figures 7A and 7B, lower panels).

### The Relationship between Direction Selectivity of Spiking and Voltage Responses

The direction selectivity of the membrane potential responses to moving gratings can be well predicted by a linear combination of the responses to stationary gratings (Jagadeesh et al., 1993, 1997) or flashing bars (Figure 3G). The direction selectivity of spiking responses, however, cannot be accounted for by linear models (Baker, 2001; DeAngelis et al., 1993; Emerson, 1997; Emerson and Huang, 1997; McLean et al., 1994). In most cells, the spike response to gratings is far more direction selective than what is predicted from a linear combination of the responses to stationary gratings or bars (Conway and Livingstone, 2003; DeAngelis et al., 1993; Reid et al., 1991). The most likely explanation for the nonlinear behavior of the spike rate responses to moving stimuli is the spike threshold. The so-called "iceberg effect" generated by a nonlinear (expansive) threshold likely enhances the difference in the spike rate responses to the two directions of grating motion relative to the difference in the membrane potential responses.

This enhancement of directionality in spiking relative to membrane potential is shown for our sample of cells in Figure 8I. Membrane potential direction indices were, in every case, much lower than spike rate indices. To determine whether the threshold nonlinearity could account quantitatively for this difference, we first modeled threshold by fitting the scatterplot of membrane potential against spike rate to a power law (Anderson et al., 2000b; Hansel and van Vreeswijk, 2002; Miller and Troyer, 2002; Priebe et al., 2004):

$$R(V_m) = k[V_m - V_{rest}]_+^p . \quad (2)$$

Data for the scatterplots in Figures 8D and 8H were taken from the responses to gratings of all different orientations and spatial frequencies and from the responses to white noise stimuli. Examples are shown in Figures 8A–8D and 8E–8H for two cells, which had exponents ($p$) of 3.05 and 3.73. We then used the power law model to predict the firing rate of the neuron in response to drifting gratings: at each point in the responses to preferred and null motion we raised the

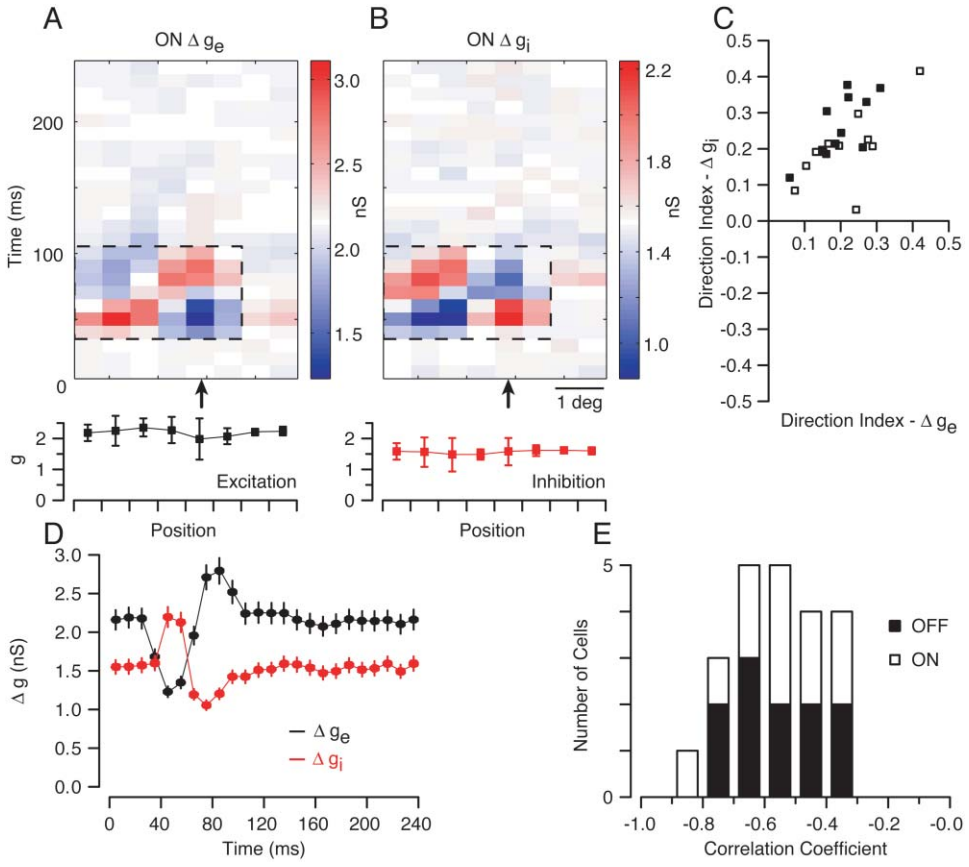


Figure 7. The Relationship between Excitation and Inhibition in X-T Maps

(A and B) An example x-t map for excitatory and inhibitory conductance recorded from a neuron with $Cs^+$ methanesulfanate and QX-314 in the recording pipette. The lower panels plot the average excitatory or inhibitory conductance at each spatial position during the epoch indicated by the dashed lines in the x-t maps. Bars indicate the standard deviation. (C) Traces in time of the $\Delta g_e$ and $\Delta g_i$ are plotted from the ON maps shown in panels (A) and (B). The spatial position of the traces is indicated by the arrows in panels (A) and (B). Bars on the traces indicate the 95% confidence intervals computed using a bootstrap procedure. (D) The correlation coefficient between x-t maps for excitatory and inhibitory conductance maps. For each neuron, the correlation coefficient was computed for the ON x-t maps (open bars) and OFF x-t maps (filled bars). The correlation coefficient was computed from the region of the map in which the variance of the conductance was significantly greater than the variance found at latencies between 0 and 20 ms. For the example neuron in panels (A) and (B), the significant region is illustrated by the dashed line. The correlation coefficient for those ON conductance x-t maps in panels (A) and (B) was −0.77. (E) The direction index estimated from each excitatory conductance x-t maps is plotted against the direction index estimated from the corresponding inhibitory conductance x-t map. Each neuron is represented by two symbols: an open symbol corresponding to the direction indices computed from the ON x-t maps and a closed symbol corresponding to the direction indices computed from OFF x-t maps.

membrane potential (Figures 8A and 8E), relative to rest, to the corresponding exponent. The resulting prediction of spike rate is shown in Figures 8C and 8G. The power law accentuates the difference between the hyperpolarizing and depolarizing phases of the responses, sharpening the response in time and increasing the direction selectivity. Note that the predicted spiking responses closely resemble the measured spiking responses (Figures 8B and 8C and 8F and 8G). For the neuron in the left column, the potential direction index of 0.36 was transformed by the power law model to a predicted value of 0.74, compared to the measured spiking direction index of 0.80. Similarly for the neuron in middle column, the potential direction index of 0.17 was transformed by the power law into a predicted spiking direction index of 0.62, compared to the measured value of 0.68.

The correlation between the measured and predicted spiking index for 23 cells was 0.79 (Figure 8J). Note that the four neurons with poorest fits by the model had measured spiking direction indices near or at 1. Since the power law model predicts spiking responses for even very small voltages above rest (unlike a threshold-linear model), a predicted direction index of 1 could only occur if the membrane potential response in the null direction always stayed at or below the resting potential, which did not occur in any of these cases. A threshold-linear model of spike rate could potentially predict the responses of these cells more accurately. Overall, however, Figure 8J suggests that an expansive voltage-to-spiking relationship, together with a linear summation of synaptic inputs, can account extremely well for the direction selectivity of simple cells as measured from their spike outputs.

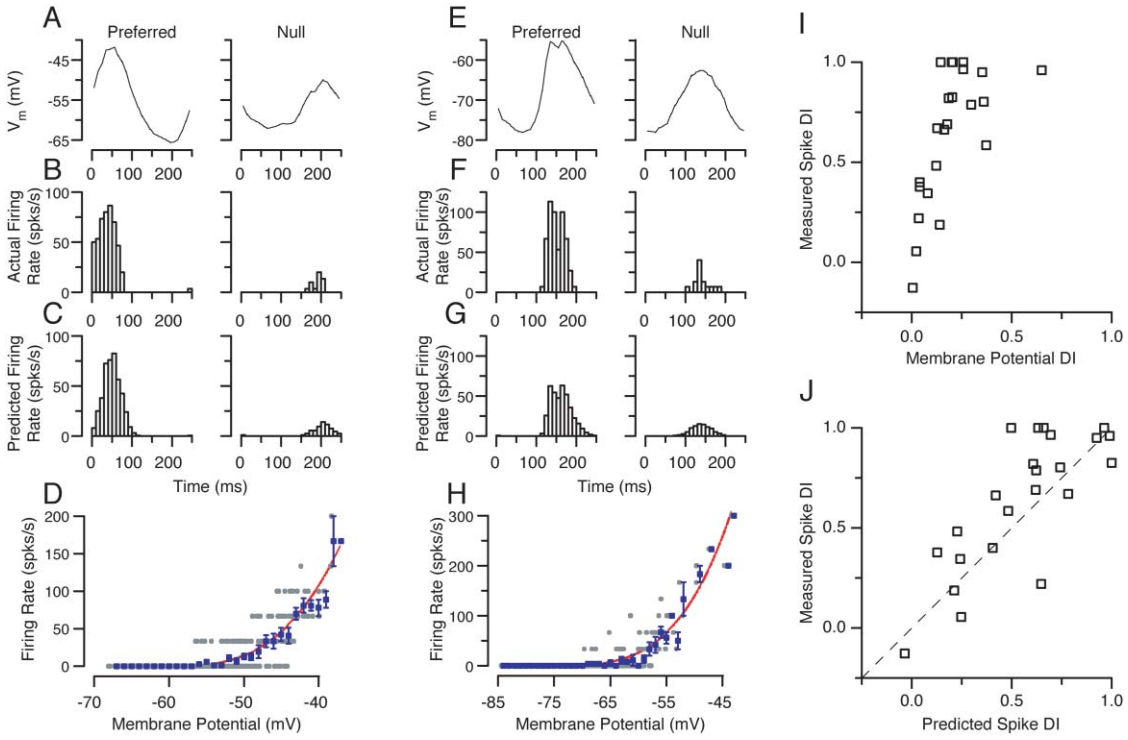


Figure 8. The Relationship between Membrane Potential and Firing Rate

The membrane potential (A) and firing rate (B) are shown for an example neuron to a grating moving in the preferred direction (left panel) and the null direction (right panel). (C) The predicted firing rate derived by applying the membrane potential response to the fitted relationship between membrane potential and firing rate. (D) The relationship between membrane potential and firing rate was fit by a power law model. Single points show the mean membrane potential and spike rate for 30 ms epochs. The blue squares show the average firing rate for membrane potentials within a 1 mV bin. Error bars are the standard error of the mean. The red curve shows the power law fit to the data. Panels (E)–(H) follow the same format as (A)–(D) for a second example neuron. (I) The direction index computed from the F1 of the spiking response is plotted against the direction index computed from the F1 of the membrane potential response. Each symbol represents the relationship for a single neuron. (J) The direction index computed from the F1 of the spiking response is compared to the F1 computed from the spiking response predicted from the membrane potential and the power law nonlinearity. The dashed trace indicates a line of slope of 1 and y-intercept of 0.

### A Comparison of Response Field Maps Derived from Spiking and Voltage Responses

The discrepancy found between spike and membrane potential direction selectivity to grating stimulation was not found when we examined direction selectivity predicted from x-t maps. We were able to construct spatiotemporal receptive field maps from the spiking responses to noise stimuli for 13 neurons with sufficiently high spike rates and long-duration recordings. Spiking response fields are remarkably similar to the voltage response fields (Figures 9A and 9B). The average correlation coefficient between voltage and spiking maps was 0.82 (std = 0.08). The direction selectivity estimated by Fourier transformation of the spiking response fields was very similar to that derived from the voltage response fields, whether measured from the ON or OFF fields alone (Figure 9C, regression slope = 0.91, not significantly different from 1, y-intercept = 0.0), or the difference between the ON and OFF fields (data not shown). The similarity between the maps based on membrane potential and maps based on spiking is consistent with the theoretical finding that a static nonlinearity should not distort a linear estimate of the receptive field as long as the stimulus is composed of Gaussian noise (Rieke, 1997). Since the 1D noise stimulus used here is a close approximation to Gaussian noise, the threshold nonlinearity would not be expected to alter the spatiotemporal receptive field.

### Discussion

It has been proposed in several models of primary visual cortex that inhibition from the nonpreferred direction is required to create direction-selective responses. In this paper, we provide evidence that the excitatory and inhibitory synaptic inputs to simple cells prefer motion in the same direction, which is the direction that evokes the most spikes. While excitation and inhibition were tuned to the same direction, the two components were evoked asynchronously by moving stimuli. This difference in the timing of excitation and inhibition appeared in responses to simple gratings as a 180° phase difference between the excitatory and inhibitory inputs. In the responses to 1D noise, the difference in timing appeared as an anticorrelation between the spatiotemporal profiles of excitation and inhibition.

The spatiotemporal relationship between excitation and inhibition for direction-selective neurons is reminis-

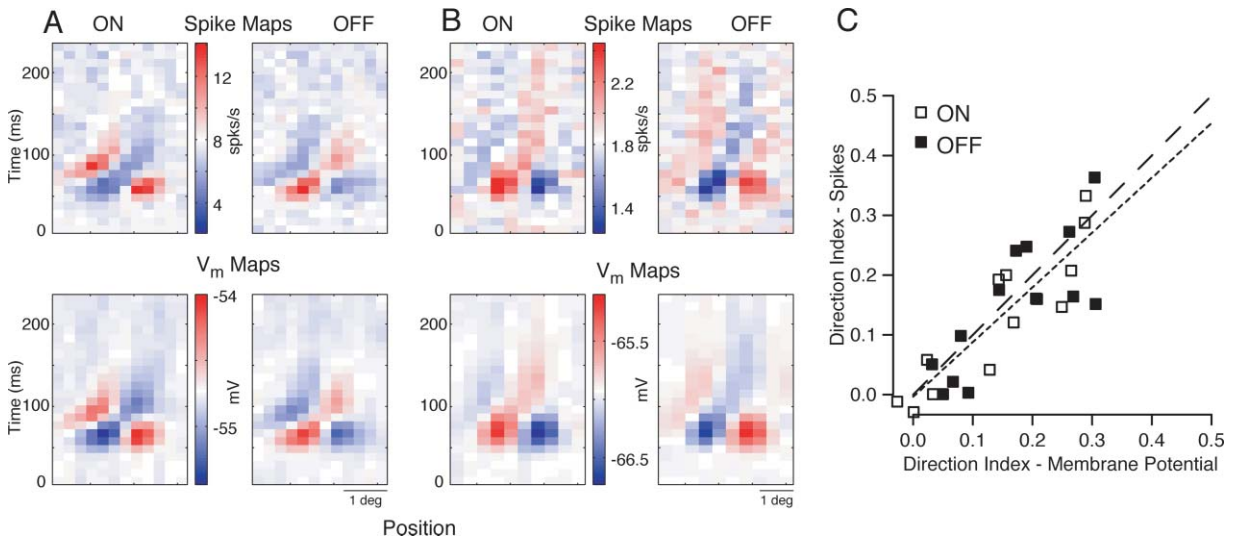


Figure 9. A Comparison of Spiking and Membrane Potential X-T Maps

(A and B) Spiking and membrane potential x-t maps are illustrated for two neurons. The top row shows x-t maps of the average firing rate after either a light bar (left panel) or dark bar (right panel). The bottom row shows membrane potential x-t maps for the same neurons. (C) The direction index extracted from membrane potential x-t maps and spiking x-t maps is shown for all 13 neurons in our dataset. Open symbols correspond to direction index extracted from the ON x-t maps, and closed symbols correspond to the OFF x-t maps. The fine dashed line indicates the regression fit to the data (slope = 0.91, y-intercept = 0.0). The thick dashed line indicates a line of slope 1 and y-intercept of 0.

cent of the push-pull arrangement of synaptic inputs thought to underlie orientation selectivity (Hirsch et al., 1998; Movshon et al., 1978; Troyer et al., 1998). A push-pull arrangement is one in which a bright bar in an ON region causes a depolarization (or "push"), while a dark bar placed in the same location causes a hyperpolarization (or "pull"). Similarly, we found that dark bars in OFF regions cause push, and bright bars cause pull. Spatiotemporal profiles such as those in Figures 6 and 7 demonstrate that push-pull interactions within direction-selective simple cell receptive fields are not solely spatial, but also extend into the temporal domain.

As previously observed in the direction-selective simple cells, we have found that voltage responses interact in a highly linear fashion (Jagadeesh et al., 1993, 1997). Responses to 1D noise showed a linear dependence on the correlation between stimulus and spatiotemporal receptive field. That is, the response to an arbitrary combination of bar stimuli closely approximated the sum of the responses to each of the component bars presented individually. Linearity was observed both for net depolarizing responses and net hyperpolarizing responses. Only at the highest levels of depolarization or hyperpolarization did linearity start to fail and saturation occur (Figure 5). Saturation in the depolarizing direction might arise from the activation of voltage-gated conductances related to spiking (Hodgkin and Huxley, 1952). Nonlinearity could also arise at the larger levels of depolarizations if the visually evoked conductance changes cause significant changes in a cell's input resistance (BorgGraham et al., 1998; Koch et al., 1983; Rall, 1964). Saturation in the hyperpolarizing direction might arise from the changes in driving force on inhibitory currents that occur as the membrane potential approaches the inhibitory reversal potential. Except for a significant range of potentials above and below rest, linearity was observed.

In contrast to the membrane potential, the spike output of direction-selective cells is highly nonlinear: the response to drifting gratings cannot be predicted from the response to stationary stimuli (DeAngelis et al., 1993; Emerson and Huang, 1997; Jagadeesh et al., 1997; Reid et al., 1987, 1991). It has been proposed that the nonlinear combination of signals occurs at a stage prior to their integration on the membrane potential through mechanisms by which inhibitory synaptic inputs block excitatory inputs from reaching the cell (Barlow and Levick, 1965; Reichardt et al., 1983; Torre and Poggio, 1978). Presynaptic inhibition or shunting inhibition could perform such a function. Our results suggest that the nonlinearity underlying direction selectivity instead occurs at the output stage of the neuron and that prior to this stage the synaptic inputs are combined in a linear fashion. As a result, the membrane potential responses to gratings can be accurately predicted from a linear transformation of the spatiotemporal receptive field. Consistent with previous proposals (Baker, 2001; Barlow and Levick, 1965; DeAngelis et al., 1993; Jagadeesh et al., 1993, 1997; McLean et al., 1994; Reichardt et al., 1983), we have demonstrated that threshold can indeed account for the nonlinear transformation between membrane potential and firing rate. Here, we have used a power law model fit to the relationship between membrane potential and spiking (Anderson et al., 2000b; Hansel and van Vreeswijk, 2002; Miller and Troyer, 2002; Priebe et al., 2004). These authors have shown that trial-to-trial variability in the spike rate associated with a given membrane potential (Azouz and Gray, 2003) smoothes the threshold-linear relationship intrinsic to the spike mechanism. The power law nonlinearity applied to measured voltage responses accounted for 82% of the variance in the spike responses. Other expansive relationships between membrane potential and spike rate, such as the

threshold-gain model (Azouz and Gray, 2003; Carandini and Ferster, 2000; Contreras and Palmer, 2003), should also be able to account for the data. But while the exact mathematical form of the nonlinearity used is not likely to be critical, the presence of some form of expansive nonlinearity is critical to the generation of strongly direction-selective spike responses.

Our results suggest that inhibition plays little role in shaping direction selectivity in simple cells. It is unclear, however, why inhibition should come from the same direction as excitation, although shared tuning for excitation and inhibition is found for other visual stimulus parameters (Anderson et al., 2000a; Ferster, 1986; Monier et al., 2003) and in other sensory modalities (Tan et al., 2004; Wehr and Zador, 2003; Zhang et al., 2003). For non-direction-selective simple cells, excitation and inhibition follow the time course of response observed here: the time of the greatest excitation is also the time of the smallest inhibition (Anderson et al., 2000a). Such push-pull interactions have also been found by spatially mapping the excitatory and inhibitory receptive fields of neurons (Ferster, 1988; Hirsch et al., 1998). One potential effect of the shared tuning of excitation and inhibition is the maintenance of linearity, such that the response to a negative (OFF) stimulus evokes the opposite of the response to a positive (ON) stimulus.

Most models of direction selectivity are based on input that differs in latency for different spatial positions (McLean and Palmer, 1989; McLean et al., 1994; Reid et al., 1987; Saul, 1995). The fundamental discrepancy has been the source of the nonlinear step that sharpens direction selectivity. While we have demonstrated that the nonlinear step occurs after the synaptic integration of input and can be accounted for by the nonlinear transformation between membrane potential and firing rate, such a nonlinear step is nonetheless required to account for direction selectivity. Since we have found that inhibition is tuned for direction, but was not largest in response to gratings moving in the null direction, inhibition could not be the basis for direction selectivity as outlined by Barlow and Levick (1965) for the retina. We focused here exclusively on simple cells since they are believed to be the first stage of cortical motion processing. It remains to be seen whether in direction-selective complex cells inhibition is tuned for the preferred or null direction.

## Experimental Procedures

### Physiological Preparation

Intracellular whole-cell electrode recordings were made in the primary visual cortex of anesthetized, paralyzed female cats (2–2.5 kg). Anesthesia was induced either with ketamine (5–15 mg/kg) and acepromazine (0.7 mg/kg) or with halothane (2%). Cannulae were then inserted into the saphenous veins and the trachea. After intravenous administration of sodium thiopental (10–20 mg/kg), the animal's head was fixed in a stereotaxic frame. Two additional measures were taken to increase the stability of recordings: (1) the animal's thoracic vertebrae were suspended from the stereotaxic frame, and (2) a pneumothoracotomy was performed. The animal was maintained under anesthesia using an intravenous infusion of sodium thiopental (1–2 mg/kg/hr) for the duration of the experiment. To minimize drift in eye position, paralysis was maintained with an infusion of either vecuronium bromide (Norcuron, 0.2 mg/kg/hr) or gallamine triethiodide (10 mg/kg/hr). Body temperature was kept at 38.3°C with a thermostatically controlled heat lamp. The electrocardiogram, electroencephalogram, autonomic signs, and body temperature were continuously monitored and recorded to ensure the anesthetic and physiological state of the animal. The nictitating membranes were retracted with phenylephrine hydrochloride, and the pupils were dilated with topical atropine. The corneas were protected by contact lenses with artificial pupils (4 mm diameter). Supplementary lenses were selected by direct ophthalmoscopy to focus the display screen onto the retina.

Borosilicate glass electrodes (A-M Systems, Carlsborg, WA) were filled in most experiments with a $K^+$-gluconate solution that included $Ca^{2+}$ buffers, pH buffers, and cyclic nucleotides. In some experiments, $K^+$-gluconate was replaced with $Cs^+$-methanesulfonate, and QX-314 (5 mM, Sigma-Aldrich) was added to the solution. Electrodes were advanced into the cortex (area 17, about 2 mm lateral of the midline) with a motorized microdrive (Sutter Instruments, Novato, CA). After the electrode was in place, warm agarose solution (3% in normal saline) was placed over the craniotomy to protect the surface of the cortex and reduce pulsations. All neurons included in this study were recorded between 480 to 900 μm from the cortical surface.

All procedures were approved by the Northwestern University Animal Care and Use Committee.

### Stimulus Presentation and Data Acquisition

Visual stimuli were generated by a Macintosh computer using the Psychophysics toolbox (Brainard, 1997; Pelli, 1997) for Matlab (Natick, MA) and presented on a ViewSonic video monitor placed 48 cm from the cat's eyes. The video monitor had a noninterlaced refresh rate of 100 Hz and a spatial resolution of 1024 × 768 pixels, which subtended 40 cm horizontally and 30 cm vertically. The video monitor had a mean luminance of 20 cd/cm$^2$.

Grating stimuli were presented for 4 s, preceded and followed by 250 ms blank (mean luminance) periods. Orientation and spatial-frequency tuning curves were made for each cell, and subsequent measures of direction selectivity were performed at the optimal orientation, spatial frequency, and spatial position. Gratings were presented at a temporal frequency of either 2 or 4 Hz. A 1D noise stimulus, composed of optimally oriented bars, was used to map the spatial and temporal components of the receptive field (DeAngelis et al., 1993). At each frame refresh of the video screen, each bar was independently set to be either bright (twice mean luminance), dark (0 luminance), or gray (mean luminance), with probabilities of 25%, 25%, and 50%. (For a few neurons, the probability of the bar being gray was higher, and the probabilities of light and dark correspondingly lower.) White noise sequences lasted for 20 s and were repeated between 8 and 135 times for each cell.

The voltage response of neurons was sampled at either 16000 or 4096 Hz and stored for subsequent analysis. Data were analyzed online to determine when enough trials had been performed to yield mean responses with low noise. Membrane potential responses were passed through a 5 ms median filter to remove action potentials (Jagadeesh et al., 1997) and were binned at the monitor frame duration (10 ms). The first cycle of response to moving gratings was discarded. The average number of presentations for each motion direction was 8.2. Since each 4 s trial contained 15 cycles of response (after discarding the first cycle), average responses were based on about 60 or 120 cycles of response, for temporal frequencies of 2 or 4 Hz, respectively.

Only neurons classified as simple were included in this dataset. Simple cells were identified by the F1/F0 ratio of the membrane potential response to optimal drifting gratings (Carandini and Ferster, 2000). That is, cells were classified as simple if the peak-to-peak amplitude of the modulated voltage response (F1) was at least 1/2 the size of the F0 (DC) component (Priebe et al., 2004). In addition, simple cells were identified by the presence of strongly segregated ON and OFF response fields.

Details of the conductance measurement method are given in the Supplemental Data (http://www.neuron.org/cgi/content/full/45/1/133/DC1/). These methods differed from previous work (Anderson et al., 2000a) in that the full membrane equation, including the $C_m dV_m/dt$ term, was used to derive conductance:

$$C_m \frac{dV_m}{dt} = -[g_e(V_m - V_e) + g_i(V_m - V_i) + g_{leak}(V_m - V_{rest})] + I_{inj} \quad (3)$$

This modification of the method to extract conductances was necessary since responses to flashing bars are more rapid than responses to drifting gratings used in previous experiments, so that the $C_m dV_m/dt$ term is no longer negligible. The membrane equation relates the capacitance and the change in membrane potential to all of the currents entering the neuron. For simplicity, we use only three conductances: excitation ($g_e$), inhibition ($g_i$), and a steady leak ($g_{leak}$). Reversal potentials for excitation and inhibition ($V_e$ and $V_i$) were taken to be 0 and −85 mV. The reversal potential for inhibition is meant to represent the combined action of $GABA_a$ and $GABA_b$. Our results do not change if the inhibitory reversal potential was assumed to be −75 mV, although the relative amplitudes of the excitatory and inhibitiory conductances do change slightly. For neurons recorded with $Cs^+$-methanesulfanate, the reversal potential for inhibition was set to −70 mV (see the Supplemental Data [http://www.neuron.org/cgi/content/full/45/1/133/DC1/]). The resting potential of the neuron was estimated from the average potential recorded in response to a gray (mean luminance) screen. The $V_m$ and $dV_m/dt$ terms in the membrane equation were taken from the recorded membrane potential and the first derivative of the membrane potential. Note that because of the background activity, the "leak" current contains both excitatory and inhibitory synaptic inputs. The estimates of excitatory and inhibitory conductance in Equation 3 are therefore not absolute estimates of excitation and inhibition, but are changes in excitatory and inhibitory conductances measured relative to the background and are referred to below as $\Delta g_e$ and $\Delta g_i$.

One potential weakness of this method of extracting visually evoked synaptic conductances is the possible activation of voltage-sensitive currents, which would distort the estimation of synaptic conductances (see Figure 4, for example). To minimize the possible effects of voltage-sensitive currents, hyperpolarizing currents were primarily used to measure conductance. Two methods were used to determine whether active currents were distorting our measurements of synaptic conductance. First, we measured the accuracy with which the measured potentials could be reconstructed from the derived currents when assuming a linear combination of synaptic inputs. Strong nonlinearities introduced by active currents would degrade the reconstruction (see the Supplemental Data [http://www.neuron.org/cgi/content/full/45/1/133/DC1/]). Second, in a number of cells, active currents were blocked by cesium and QX-314. Both methods suggest that our measurements of conductance are appropriate.

## Acknowledgments

We thank C.E. Boudreau, I. Finn, I. Lampl, and H. Ozeki for useful conversations. Supported by grants from the National Institute of Health (EY-014499 and EY-04726).

Received: August 2, 2004
Revised: September 29, 2004
Accepted: November 15, 2004
Published: January 5, 2005

## References

Adelson, E.H., and Bergen, J.R. (1985). Spatiotemporal energy models for the perception of motion. J. Opt. Soc. Am. A. *2*, 284–299.

Anderson, J.C., Binzegger, T., Kahana, O., Martin, K.A., and Segev, I. (1999). Dendritic asymmetry cannot account for directional responses of neurons in visual cortex. Nat. Neurosci. *2*, 820–824.

Anderson, J.S., Carandini, M., and Ferster, D. (2000a). Orientation tuning of input conductance, excitation, and inhibition in cat primary visual cortex. J. Neurophysiol. *84*, 909–926.

Anderson, J.S., Lampl, I., Gillespie, D.C., and Ferster, D. (2000b). The contribution of noise to contrast invariance of orientation tuning in cat visual cortex. Science *290*, 1968–1972.

Azouz, R., and Gray, C.M. (2003). Adaptive coincidence detection and dynamic gain control in visual cortical neurons in vivo. Neuron *37*, 513–523.

Baker, C.L., Jr. (2001). Linear filtering and nonlinear interactions in direction-selective visual cortex neurons: a noise correlation analysis. Vis. Neurosci. *18*, 465–485.

Barlow, H.B., and Levick, R.W. (1965). The mechanism of directional selectivity in the rabbit's retina. J. Physiol. *173*, 377–407.

BorgGraham, L.J., Monier, C., and Fregnac, Y. (1998). Visual input evokes transient and strong shunting inhibition in visual cortical neurons. Nature *393*, 369–373.

Brainard, D.H. (1997). The psychophysics toolbox. Spat. Vis. *10*, 433–436.

Carandini, M., and Ferster, D. (2000). Membrane potential and firing rate in cat primary visual cortex. J. Neurosci. *20*, 470–484.

Contreras, D., and Palmer, L. (2003). Response to contrast of electrophysiologically defined cell classes in primary visual cortex. J. Neurosci. *23*, 6936–6945.

Conway, B.R., and Livingstone, M.S. (2003). Space-time maps and two-bar interactions of different classes of direction-selective cells in macaque V-1. J. Neurophysiol. *89*, 2726–2742.

DeAngelis, G.C., Ohzawa, I., and Freeman, R.D. (1993). Spatiotemporal organization of simple-cell receptive fields in the cat's striate cortex. II. Linearity of temporal and spatial summation. J. Neurophysiol. *69*, 1118–1135.

Emerson, R.C. (1997). Quadrature subunits in directionally selective simple cells: spatiotemporal interactions. Vis. Neurosci. *14*, 357–371.

Emerson, R.C., and Huang, M.C. (1997). Quadrature subunits in directionally selective simple cells: counterphase and drifting grating responses. Vis. Neurosci. *14*, 373–385.

Emerson, R.C., Citron, M.C., Vaughn, W.J., and Klein, S.A. (1987). Nonlinear directionally selective subunits in complex cells of cat striate cortex. J. Neurophysiol. *58*, 33–65.

Ferster, D. (1986). Orientation selectivity of synaptic potentials in neurons of cat primary visual cortex. J. Neurosci. *6*, 1284–1301.

Ferster, D. (1988). Spatially opponent excitation and inhibition in simple cells of the cat visual cortex. J. Neurosci. *8*, 1172–1180.

Ferster, D., and Miller, K.D. (2000). Neural mechanisms of orientation selectivity in the visual cortex. Annu. Rev. Neurosci. *23*, 441–471.

Ferster, D., Chung, S., and Wheat, H. (1996). Orientation selectivity of thalamic input to simple cells of cat visual cortex. Nature *380*, 249–252.

Grzywacz, N.M., and Koch, C. (1987). Functional properties of models for direction selectivity in the retina. Synapse *1*, 417–434.

Hansel, D., and van Vreeswijk, C. (2002). How noise contributes to contrast invariance of orientation tuning in cat visual cortex. J. Neurosci. *22*, 5118–5128.

Hirsch, J.A., Alonso, J.M., Reid, R.C., and Martinez, L.M. (1998). Synaptic integration in striate cortical simple cells. J. Neurosci. *18*, 9517–9528.

Hodgkin, A.L., and Huxley, A.F. (1952). A quantitative description of membrane current and its application to conduction and excitation in nerve. J. Physiol. *117*, 500–544.

Jagadeesh, B., Wheat, H.S., and Ferster, D. (1993). Linearity of summation of synaptic potentials underlying direction selectivity in simple cells of the cat visual cortex. Science *262*, 1901–1904.

Jagadeesh, B., Wheat, H.S., Kontsevich, L.L., Tyler, C.W., and Ferster, D. (1997). Direction selectivity of synaptic potentials in simple cells of the cat visual cortex. J. Neurophysiol. *78*, 2772–2789.

Koch, C., Poggio, T., and Torre, V. (1983). Nonlinear interactions in a dendritic tree: localization, timing, and role in information processing. Proc. Natl. Acad. Sci. USA *80*, 2799–2802.

McCormick, D.A., Connors, B.W., Lighthall, J.W., and Prince, D.A. (1985). Comparative electrophysiology of pyramidal and sparsely spiny stellate neurons of the neocortex. J. Neurophysiol. *54*, 782–806.

McLean, J., and Palmer, L.A. (1989). Contribution of linear spatiotemporal receptive field structure to velocity selectivity of simple cells in area 17 of cat. Vision Res. *29*, 675–679.

McLean, J., Raab, S., and Palmer, L.A. (1994). Contribution of linear mechanisms to the specification of local motion by simple cells in areas 17 and 18 of the cat. Vis. Neurosci. *11*, 271–294.

Miller, K.D., and Troyer, T.W. (2002). Neural noise can explain expansive, power-law nonlinearities in neural response functions. J. Neurophysiol. *87*, 653–659.

Monier, C., Chavane, F., Baudot, P., Graham, L.J., and Fregnac, Y. (2003). Orientation and direction selectivity of synaptic inputs in visual cortical neurons: a diversity of combinations produces spike tuning. Neuron *37*, 663–680.

Movshon, J.A., Thompson, I.D., and Tolhurst, D.J. (1978). Spatial summation in the receptive fields of simple cells in the cat's striate cortex. J. Physiol. *283*, 53–77.

Pelli, D.G. (1997). The VideoToolbox software for visual psychophysics: transforming numbers into movies. Spat. Vis. *10*, 437–442.

Priebe, N.J., Mechler, F., Carandini, M., and Ferster, D. (2004). The contribution of spike threshold to the dichotomy of cortical simple and complex cells. Nat. Neurosci. *7*, 1113–1122.

Rall, W. (1964). Theoretical significance of dendritic trees for neuronal input-output relations. In Neural Theory and Modeling, R.R. Stanford, ed. (Stanford: Stanford Univ. Press), pp. 73–97.

Reichardt, W., Poggio, T., and Hausen, K. (1983). Figure-ground discrimination by relative movement in the visual system of the fly. Biol. Cybern. *46*, 1–30.

Reid, R.C., Soodak, R.E., and Shapley, R.M. (1987). Linear mechanisms of directional selectivity in simple cells of cat striate cortex. Proc. Natl. Acad. Sci. USA *84*, 8740–8744.

Reid, R.C., Soodak, R.E., and Shapley, R.M. (1991). Directional selectivity and spatiotemporal structure of receptive fields of simple cells in cat striate cortex. J. Neurophysiol. *66*, 505–529.

Rieke, F. (1997). Spikes: Exploring the Neural Code (Cambridge, MA: MIT Press).

Saul, A.B. (1995). Adaptation aftereffects in single neurons of cat visual cortex: response timing is retarded by adapting. Vis. Neurosci. *12*, 191–205.

Saul, A., and Humphrey, A. (1990). Spatial and temporal response properties of lagged and nonlagged cells in cat lateral geniculate nucleus. J. Neurophysiol. *64*, 206–224.

Saul, A.B., and Humphrey, A.L. (1992). Evidence of input from lagged cells in the lateral geniculate nucleus to simple cells in cortical area 17 of the cat. J. Neurophysiol. *68*, 1190–1208.

Sokal, R.R., and Rohlf, F.J. (1995). Biometry: The Principles and Practice of Statistics in Biological Research, Third Edition (New York: W.H. Freeman).

Tan, A.Y., Zhang, L.I., Merzenich, M.M., and Schreiner, C.E. (2004). Tone-evoked excitatory and inhibitory synaptic conductances of primary auditory cortex neurons. J. Neurophysiol. *92*, 630–643.

Torre, V., and Poggio, T. (1978). A synaptic mechanism possibly underlying directional selectivity to motion. Proc. R. Soc. Lond. B. Biol. Sci. *202*, 409–416.

Troyer, T.W., Krukowski, A.E., Priebe, N.J., and Miller, K.D. (1998). Contrast-invariant orientation tuning in cat visual cortex: Thalamocortical input tuning and correlation-based intracortical connectivity. J. Neurosci. *18*, 5908–5927.

Wehr, M., and Zador, A.M. (2003). Balanced inhibition underlies tuning and sharpens spike timing in auditory cortex. Nature *426*, 442–446.

Zhang, L.I., Tan, A.Y., Schreiner, C.E., and Merzenich, M.M. (2003). Topography and synaptic shaping of direction selectivity in primary auditory cortex. Nature *424*, 201–205.